On the catalytic transfer hydrogenation of nitroarenes by a cubane-type Mo_3S_4 cluster hydride: Disentangling the nature of the reaction mechanism†

Vicent S. Safont,[1,*] Iván Sorribes,[1] Juan Andrés,[1] Rosa Llusar,[1] Mónica Oliva,[1] Maxim R. Ryzhikov[1,2]

[1] Departament de Química Física i Analítica, Universitat Jaume I, Av. Sos Baynat s/n, 12071 Castelló, Spain

[2] Nikolaev Institute of Inorganic Chemistry, Siberian Branch of the Russian Academy of Sciences, 3 Lavrentiev av., Novosibirsk, 630090, Russia

† Electronic supplementary information (ESI) available: basis set test, temperature influence, comparison between theoretical levels, non-catalytic reduction of nitrobenzene to aniline, multiple metal centre mechanism, and energies and Cartesian coordinates of the optimized species.

Corresponding author: Vicent S. Safont e-mail: safont@uji.es

This work is dedicated to the memory of professor Juan Murga Clausell

KEYWORDS: nitroarenes reduction mechanism, catalysis, molybdenum sulphides, cluster

Abstract

Cubane-type Mo_3S_4 cluster hydrides decorated with phosphine ligands are active catalysts for the transfer hydrogenation of nitroarenes to aniline derivatives in the presence of formic acid (HCOOH) and triethylamine (Et_3N). The process is highly selective and most of the cluster species involved in the catalytic cycle have been

identified through reaction monitoring. Formation of a dihydrogen cluster intermediate has also been postulated based on previous kinetic and theoretical studies. However, the different steps involved in the transfer hydrogenation from the cluster to the nitroarene to finally produce aniline remain unclear. Herein, we report an in-depth computational investigation into this mechanism. Et_3N reduces the activation barrier associated with the formation of Mo-H···HOOCH dihydrogen species. The global catalytic process is highly exergonic and occurs in three consecutive steps with nitrosobenzene and phenylhydroxylamine as reaction intermediates. Our computational findings explain how hydrogen is transferred from these Mo-H···HOOCH dihydrogen adducts to nitrobenzene with the concomitant formation of nitrosobenzene and the formate substituted cluster. Then, a β-hydride elimination reaction accompanied by CO_2 release regenerates the cluster hydride. Two additional steps are needed for hydrogen transfer from the dihydrogen cluster to nitrosobenzene and phenylhydroxylamine to finally produce aniline. Our results show that the three metal centres in the Mo_3S_4 unit act independently, so the cluster can exist in up to ten different forms that are capable to open a wide range of reaction paths. This behaviour reveals the outstanding catalytic possibilities of this kind of cluster complexes, which work as highly efficient catalytic machines.

Introduction

Catalytic reduction of nitroarenes to the corresponding aniline derivatives is of crucial importance at both industrial and laboratory scale, since anilines are commonly used as building blocks in the manufacture of dyes, pigments, agrochemicals and pharmaceuticals.[1] For instance, one of the commercial routes explored for the production of paracetamol (N-acetyl-p-aminophenol, acetaminophen), an antipyretic and analgesic drug used worldwide to reduce fever, relieve coughing, colds and pain including muscular aches as well as chronic pain, involves a nitroarene reduction process as one of the key final stages.[2] Typically, catalytic hydrogenation is the preferred methodology to accomplish the nitro group reduction because the desired anilines are obtained with high atom economy.[3] However, its application involves some drawbacks, such as the cost of the high-pressure equipment and the risk of handling H_2. In addition, the typically demanded high temperatures and H_2 pressures constrain the chemoselectivity towards the nitro group hydrogenation, especially when other reducible functionalities are present. Although significant advantages in nitroarene hydrogenation reactions have been

accomplished by application of homogeneous[4] as well as heterogeneous[2c, 5] efficient catalytic systems, the chemoselectivity is still an important issue to be further improved.

Transfer hydrogenation reactions involving formic acid as a liquid surrogate of H_2 constitute an attractive alternative to well-established catalytic hydrogenations for the synthesis of valuable chemical compounds.[6] This strategy allows performing efficient and selective reductive transformations under safer and milder conditions.[7] The key to this success lies in the application of active and versatile catalysts, which should be designed on the basis of a deep understanding of the reaction steps. However, this cannot be achieved based only on heuristic experiments –instead solid mechanistic arguments are needed. For this purpose, combining experimental techniques with density functional theory (DFT) calculations provides a unified approach towards the improved design of more efficient catalysts.

Transition metal cluster complexes are relevant not only as singular catalysts due to their multiple metal-metal reactivity, but also as models of active sites of heterogeneous catalysts; therefore, a deep understanding of the processes mediated by these molecular clusters is important both in material science and catalysis.[8] Recently some of us in collaboration with Beller's group have developed a series of molybdenum cluster species which are efficient chemoselective catalysts for the reduction of nitroarenes.[4i, 7e, 9] In particular, we have shown that the trinuclear $[Mo_3S_4H_3(dmpe)_3]^+$ (dmpe = 1,2-(bis)dimethyl-phosphinoethane) cluster hydride catalyses the transfer hydrogenation of nitroarenes to anilines in the presence of an azeotropic mixture of formic acid (HCOOH) and trimethylamine (Et_3N), in tetrahydrofuran (THF) solvent at 70 ºC as the best experimental conditions.[7e] Although reaction monitoring using mass spectroscopic techniques (*vide infra*) have allowed us to identify the nature of most relevant cluster species present in the catalytic cycle, full mechanistic details on the interaction between these cluster complexes and the different organic substrates are still unclear. In this scenario, accurate computational studies emerge as a key tool for elucidating the different steps of this transfer hydrogenation mechanism.

Herein, we report a detailed theoretical study, performed at the DFT level, of the catalytic transfer hydrogenation of nitrobenzene to aniline using a phosphine Mo_3S_4 cluster hydride in the presence of HCOOH as reducing agent. The process takes place with CO_2 and H_2O formation, according to equation 1:

$$C_6H_5NO_2 + 3\ HCOOH \rightarrow C_6H_5NH_2 + 3\ CO_2 + 2\ H_2O \qquad \text{(eq. 1)}$$

After addressing the role of Et_3N in enhancing the catalyst performance of the Mo_3S_4 cluster hydride, a full description of the transfer hydrogenation mechanism is presented. In a first approach, the study is restricted to a metal centre, since metal atoms act independently according to the observed statistically controlled kinetics.[10] A full description of the elementary steps of the reaction mechanism is given. A comparison between the catalysed and non-catalysed mechanism is also provided. We then extend our calculations to three metal centres, which reveals the complex nature of the nitrobenzene to aniline reduction mediated by the Mo_3S_4 hydride complex and illustrates the extraordinary catalytic power of these cluster complexes as highly efficient catalytic machines.

Computational Details

The calculations were carried out by using the Gaussian 09 program.[11] In a first approach, the Becke hybrid density functional (B3LYP)[12] method was combined with the double-ζ pseudo-orbital basis set LanL2DZ, in which H, C and N are represented by the Dunning–Huzinaga valence double-zeta basis set[13] and P, S and Mo are represented by the relativistic core LanL2 potential of Los Alamos plus DZ.[14] B3LYP/LanL2DZ has proven to be a reliable tool for describing geometric structures and energy profiles of M_3S_4 (M = Mo, W) clusters.[15] In addition, we have tested other basis set (CEP-121G as well as Def2SVP), because of the possible B3LYP/LanL2DZ limitations due to superposition errors (see Table SI1). The free energy barrier height calculated with the Lanl2DZ basis set is *ca*. 3 kcal/mol lower that that calculated with the CEP-121G basis set, which, in turn, is *ca*. 3 kcal/mol lower than that obtained with the B3LYP/Def2SVP method (36.6 kcal/mol). On the other hand, it has been reported that B3LYP hybrid functional under-estimates hydrogen bond strengths, and consistently over-estimates hydrogen bond lengths.[16] Therefore, as several hydrogen transfers along hydrogen bonds are suggested to take place in the reactions herein studied, we have used the Becke88 (B)[17] gradient-corrected exchange functional combined with the Perdew86 (P86)[18] gradient-corrected correlation functional. BP86 has been reported to excellently recover the experimental values for hydrogen bond lengths and strengths.[16] Hence, we used BP86 combined with a basis set (BS1) in which Mo and S atoms were described using the SDD relativistic ECP and associated basis set[19] with added polarization functions for the latter

(ζ=0.503),[20] and the remaining atoms were described with the 6-31G(d,p) basis set[21], to obtain improved energy values. As an added value, a comparison between the results obtained with the two approaches (B3LYP/LanL2DZ *vs* BP86/BS1) is also offered.

All geometry optimizations were performed without any symmetry constraints followed by analytical frequency calculations to confirm that a minimum or a transition state (TS) has been reached. The Intrinsic Reaction Coordinate paths[22] have been followed along both directions of each transition state vector to confirm the nature of the species connected by a given TS. The effects of the THF solvent were calculated by means of PCM-based model[23] at the same theoretical levels as the gas phase computations. In addition, dispersion corrections were computed for all stationary points found by using Grimme's D3 parameter set,[24] and thus the free energies shown herein include the dispersion correction as well.

In this work, DFT calculations have been carried out using $[Mo_3S_4H_3(PH_3)_6]^+$ (**1**) as a molecular model of the cubane-type $[Mo_3S_4H_3(dmpe)_3]^+$ cluster, a standard approach employed by our group when dealing with these kind of systems to attain reasonable computational times without losing the description of the reaction centres.[25] To further validate our approach, we have compared the energy associated to the **1**···HCOOH formation from **1** and HCOOH at the experimental conditions (THF solvent at 70 degrees) with the energies associated to the same process using the $[Mo_3S_4H_3(dmpe)_3]^+$ cluster. The calculated values at the BP86/BS1 level are +1.3 kcal/mol using the **1** molecular model *versus* +2.5 employing the dmpe cluster. Similar differences are found between values calculated at the B3LYP/LanL2DZ level, +3.9 kcal/mol for **1** *versus* +2.9 for the $[Mo_3S_4H_3(dmpe)_3]^+$ cluster. As the energies obtained are roughly the same for both clusters, the use of **1** as model of $[Mo_3S_4H_3(dmpe)_3]^+$ is validated.

Results and Discussion

Cubane-type M_3S_4 hydride clusters of general formula $[M_3S_4H_3(dmpe)_3]^+$ (M=Mo, W) react with HX acids to afford the corresponding substituted $[M_3S_4X_3(dmpe)_3]^+$ halide complexes.[10, 15b, 26] Stopped-flow kinetic studies in combination with DFT calculations gave support to the formation of M-H···H-X and/or M-H···H-X···H-X dihydrogen species, depending on the nature of the solvent. Consequently, first- and second-order dependences on the acid concentration were observed. In general, these substitution reactions occurred with statistically controlled kinetics, so theoretical studies on the

cluster–acid interaction could be restricted in a first approach to only a metal centre.[10] On the basis of this background and through detection of molybdenum cluster species by catalytic reaction monitoring with a pressurized sample infusion (PSI) ESI-MS technique,[27] we recently proposed a tentative catalytic cycle of the cluster species involved in the Mo_3S_4-catalysed transfer hydrogenation of nitrobenzene to aniline in the presence of a mixture of HCOOH/Et_3N as a reducing agent.[7e] As shown in Scheme 1, the reaction of the $[Mo_3S_4H_3(dmpe)_3]^+$ hydride complex with formic acid generates unstable dihydrogen species, from which hydrogen is transferred to nitrobenzene to afford the formate-substituted cluster. Then, β-hydride elimination reaction accompanied by the release of CO_2 regenerates the cluster hydride. Additional previous experimental results showed that aniline formation preferentially takes place through the direct reduction route with nitrosobenzene and phenyl hydroxylamine as reaction intermediates, thus suggesting that conversion of nitrobenzene to aniline is achieved after three consecutive catalytic cycles.[7e] It should be noted that a similar mechanism has recently been proposed by Parkin et al. for the dehydrogenation, disproportionation and transfer hydrogenation reactions of formic acid catalysed by mononuclear molybdenum hydride compounds.[28]

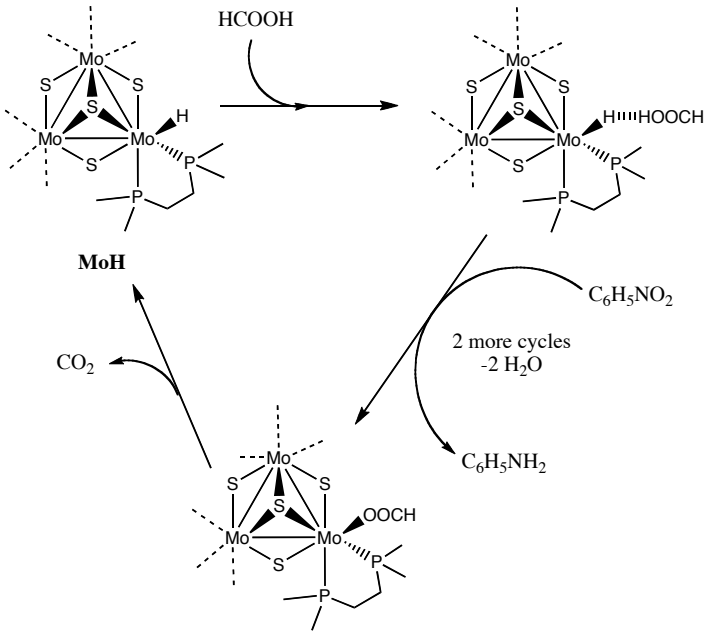

Scheme 1. Proposed catalytic cycle for the molybdenum cluster species involved in the reduction of nitrobenzene. Scheme adapted from reference 7e.

Firstly, we have focused on the role of Et_3N since previous experimental results revealed that its presence enhances catalytic performance as compared with pure formic

acid. Formic acid exists in THF solution as dimers, and the calculated free energy variation accompanying the process $(HCOOH)_2$ + **1** to yield **1**···HOOCH + HCOOH at room temperature is +7.2 (at BP86/BS1 level) kcal/mol. The presence of NEt_3 makes easier the $(HCOOH)_2$ dissociation, since the process $(HCOOH)_2$ + NEt_3 to yield HCOOH···NEt_3 + HCOOH requires only 3.9 kcal/mol, which facilitates the complex formation, because further interaction of **1** with a single HCOOH molecule to afford **1**···HOOCH occurs with a decrease in the free energy of the system of 3.9 kcal/mol, which is ca. 11.1 kcal/mol lower than that calculated for association with the $(HCOOH)_2$ dimers.

Single metal centre mechanism

In this section, we evaluate the free energy associated to the proton transfer from the activated **1**···HOOCH (**2**) adduct to nitrobenzene at one metal centre. The first reaction step of the initial cycle takes place according to equation 2 through the transition state **TS1** to afford the formate $[Mo_3S_4H_2(OCHO)(PH_3)_6]^+$ (**3**) cluster derivative, nitrosobenzene and water.

1···HOOCH (**2**) + $C_6H_5NO_2$ → $[Mo_3S_4H_2(OCHO)(PH_3)_6]^+$ (**3**) + C_6H_5NO + H_2O (eq. 2)

Figure 1 displays the optimized structures of the dihydrogen **2** adduct, transition state **TS1**, and the resulting formate cluster species **3** calculated at the BP86/BS1 level. There are not significant differences between the structures calculated at this level with those optimized using B3LYP/LanL2DZ, with root mean square deviations (RMSD) for **TS1** of 0.198 Å.

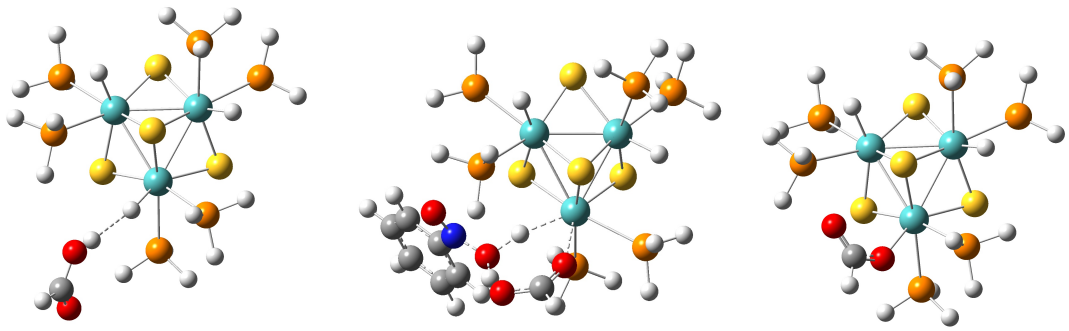

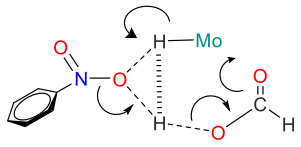

2 **TS1** **3**

Figure 1. Optimized structures of **2**, **TS1** and **3**. Blue, yellow, orange and white spheres represent the Mo, S, P and H atoms, respectively. C atoms are depicted as grey balls, the O atoms in red, and the N atom in dark blue. The inset depicts the bonds rearrangement at **TS1** (see text).

The reaction proceeds with one of the oxygen atoms of nitrobenzene roughly approaching the midpoint of the H···H fragment in **2**. This approach causes a simultaneous bond length increase in one of the nitrobenzene N-O bonds and reorientation of the formate species with one of its oxygen atoms pointing towards the metal. Transition state **TS1** describes the changes taking place in this single step process, namely, H_2O and nitrosobenzene release, and the formate-cluster formation. The large value of the **TS1** imaginary frequency (1044.8i cm^{-1}, calculated at the BP86/BS1 level in THF solvent) is associated to the dominant motion of the hydrogen atoms, particularly the H transfer from the Mo to the oxygen atom, coupled to the N-O enlargement and, to a much lesser extent, the O-C-O bending. Recovery of the catalyst during the first cycle occurs according to equation (3) via transition state **TS2** (see Figure 2) and implies the release of a CO_2 molecule.

$$[Mo_3S_4H_2(OCHO)(PH_3)_6]^+ (\mathbf{3}) \rightarrow \mathbf{1} + CO_2 \qquad \text{(eq. 3)}$$

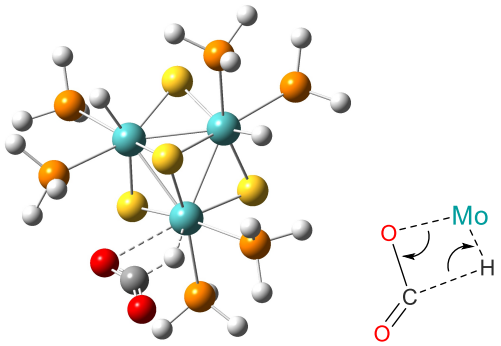

Figure 2. Structure of **TS2**. The inset depicts the bonds rearrangement at **TS2**.

From **TS2**, the original hydride catalyst **1** is recovered through an H transfer from the C atom of the formate ligand to the Mo atom accompanied by CO_2 release. The imaginary frequency for **TS2** (130.1i cm^{-1}) is one order of magnitude lower value than that computed for **TS1**. In this case, the atomic motions that dominate the transition vector correspond to Mo-O breaking, H transfer and the CO_2 linearization process.

The second catalytic cycle corresponds to the conversion of nitrosobenzene to phenyl hydroxylamine as represented in equation 4. Again, the dihydrogen cluster interacts with the organic substrate opening the pathway through **TS3,** represented in Figure 3, with the formation of phenyl hydroxylamine (C_6H_5NHOH) and the formate **3** complex.

1···HOOCH (**2**) + C_6H_5NO→ $[Mo_3S_4H_2(OCHO)(PH_3)_6]^+$ (**3**) + C_6H_5NHOH (eq. 4)

In **TS3** (see Figure 3) the N-O moiety of nitrosobenzene inserts between the hydrogen atoms of the H···H fragment in **2** while the formate ligand moves leading to the formation of a Mo-O bond to produce **3**. The imaginary frequency value is 45.3i cm^{-1}, and the main components of the transition vector (TV) are the formate ligand reorientation coupled with the hydrogen transfer from Mo to the O atom of nitrosobenzene, while the acidic proton is almost completely transferred to the N atom. As before, the formate cluster **3** undergoes decarboxylation via **TS2** to recover **1**.

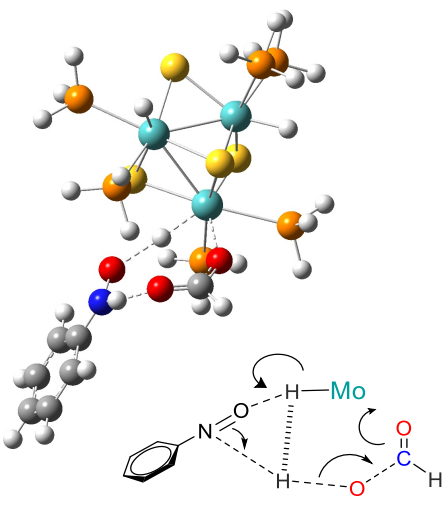

TS3

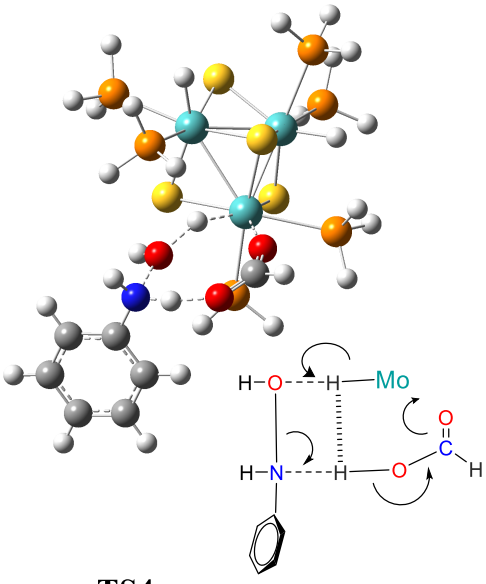

TS4

Figure 3. Structures of **TS3** and **TS4**. The insets depict the corresponding bonds rearrangements.

The last catalytic cycle involves the aniline formation from phenyl hydroxylamine, as shown in equation 5. In this step, cluster **1** is activated for a third time by a HCOOH molecule, and transfer of two hydrogen atoms occurs trough **TS4**, represented in Figure 3, to afford the amine.

$$\mathbf{1}\cdots HOOCH\ (\mathbf{2}) + C_6H_5NHOH \rightarrow [Mo_3S_4H_2(OCHO)(PH_3)_6]^+(\mathbf{3}) + C_6H_5NH_2 + H_2O \qquad \text{(eq. 5)}$$

The imaginary frequency associated to **TS4** is 577.6i cm^{-1}, and the main atomic motions that describe the TV correspond to the H transfer from Mo to the oxygen atom of phenyl hydroxylamine, coupled with the N-O bond enlargement and, to a lesser extent, with the acidic H transfer to the N atom. Thus, **TS4** describes the water and aniline release, as well as the formation of **3**. Then, **3** decarboxylates via **TS2** recovering catalyst **1** and releasing another CO_2 molecule, thus closing the three-cycle catalytic process.

Table 1 lists the Gibbs free energies for the three-cycle catalytic conversion of nitrobenzene to aniline (equation 1), calculated at the BP86/BS1 level under the experimental conditions, that is in THF and 70 ºC. The energy profile is represented in Figure 4, using the nomenclature defined in Table 1 in which the subscript numbers refer to the particular catalytic cycle. Values calculated in gas phase are also given in Table 1 for comparison.

Table 1. Gibbs free energies (kcal/mol) relative to **R** of the different stationary points calculated at the BP86/BS1 level under the experimental conditions, and in gas phase at room temperature.

Entry		THF, 70 °C	Gas Phase, RT
1	**R**: **1** + 3 HCOOH + $C_6H_5NO_2$	0.0	0.0
2	$\mathbf{2_1}$: **2** + 2 HCOOH + $C_6H_5NO_2$	1.3	-3.9
3	$\mathbf{TS1_1}$: **TS1** + 2 HCOOH	28.2	16.4
4	$\mathbf{3_1}$: **3** + 2 HCOOH + H_2O + C_6H_5NO	-30.0	-29.7
5	$\mathbf{TS2_1}$: **TS2** + 2 HCOOH + H_2O + C_6H_5NO	-6.0	-3.4
6	$\mathbf{1_1}$: **1** + 2 HCOOH + CO_2 + H_2O + C_6H_5NO	-23.4	-22.0

7	**2_2**: **2** + HCOOH + CO_2 + H_2O + C_6H_5NO	-22.1	-25.8
8	**$TS3_2$**: **TS3** + HCOOH + CO_2 + H_2O	-3.0	-14.3
9	**3_2**: **3** + HCOOH + CO_2 + H_2O + C_6H_5NHOH	-55.3	-56.6
10	**$TS2_2$**: **TS2** + HCOOH + CO_2 + H_2O + C_6H_5NHOH	-31.2	-30.3
11	**1_2**: **1** + HCOOH + 2 CO_2 + H_2O + C_6H_5NHOH	-48.6	-48.9
12	**2_3**: **2** + 2 CO_2 + H_2O + C_6H_5NHOH	-47.3	-52.8
13	**$TS4_3$**: **TS4** + 2 CO_2 + H_2O	-21.6	-31.3
14	**3_3**: **3** + 2 CO_2 + 2 H_2O + $C_6H_5NH_2$	-114.7	-113.5
15	**$TS2_3$**: **TS2** + 2 CO_2 + 2 H_2O + $C_6H_5NH_2$	-90.7	-87.2
16	**P**: **1** + 3 CO_2 + 2 H_2O + $C_6H_5NH_2$	-108.1	-105.8

Entries 1 to 6 correspond to the first cycle. Formation of the dihydrogen cluster **2** from **1** and HCOOH is slightly endergonic by 1.3 kcal/mol (entry 2, Table 1). The activation Gibbs free energy leading to **TS1** is 26.9 kcal/mol. Formation of the formate complex **3** and nitrosobenzene (labelled as $\mathbf{3_1}$) from **TS1** is calculated to be very exergonic (-58.2 kcal/mol). From this point, an energy increase of 24.0 kcal/mol leads the system to the second transition state, **TS2**, from which cluster hydride **1** regenerates. Notice that cluster **1** regeneration through **TS2** is identical for all three cycles.

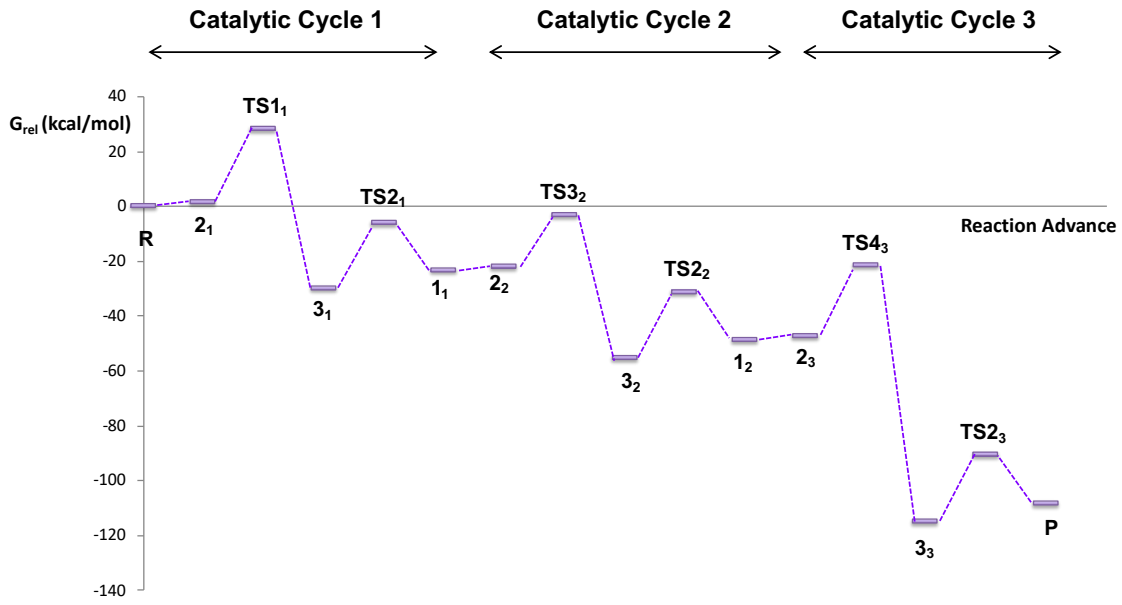

Figure 4. Gibbs free energy profile for the transfer hydrogenation to nitroarenes mediated by the hydride cluster **1**; see Table 1 for the nomenclature used.

The highest energy value along the reaction path (see Table 1 and Figure 4) corresponds to **TS1$_1$** and, once it is reached, the reaction proceeds smoothly. Free Gibbs activation energies for **TS3** (19.1 kcal/mol) and **TS4** (25.7 kcal/mol) are lower than that for **TS1**. Therefore, the rate limiting step would correspond to the hydrogen transfer to the nitroarene to form the nitrosoderivative and water (see below). Notice that the whole process is highly exergonic with a Gibbs free energy decrease of 108.1 kcal/mol.

An analysis of the results renders that a moderate initial input of energy (28.2 kcal/mol) is needed to engage the catalytic transfer hydrogenation, likely associated to the temperature needed (70 ºC) to start the process. Once **TS1$_1$** has been surmounted, the system evolves to reach the final products, in concordance with the experimental results, in which no accumulation of organic intermediates is detected.[7e] As shown in Figure 4, the system can have some tendency to accumulate **3$_3$**, *i.e.,* the formate complex **3** plus aniline. This is in agreement with the experimental detection of small quantities of the monoformate cluster at short reaction times, whereas at longer reaction times, the triformate cluster form is detected (see below).

The data reported in Table 1 show that the inclusion of the solvent in the calculations does not have a significant effect on the whole thermodynamic description of the process, as expected for a solvent of low polarity as THF. However, there is an increase of the relative Gibbs free energy of **TS1**, **TS3** and **TS4**. This fact can be understood due to the larger stabilization of the separated molecules, cluster, HCOOH and the aromatic species which are much more accessible to the THF than the TSs. On the other hand, the increase of the Gibbs free energy for TSs is also partly due to the temperature (see Table SI2 for the temperature effect in gas phase), and is associated to the entropy decrease when the cluster, HCOOH and the aromatic species join together for the process to take place. Hence, the unfavourable entropic term increases its influence in the ΔG values for TSs as the temperature raises.

Experimental conditions for reaction completion (3 mol% of catalyst loading in 10 h) correspond to an average turnover frequency (TOF) of 3.33 h^{-1} ($9.26 \cdot 10^{-4}$ s^{-1}). From this value, an energetic span (δE) of *ca* 25 (24.9) kcal/mol can be estimated using the simplified Eyring equation (eq. 6),[29]

$$\mathrm{TOF} = \frac{k_B T}{h} e^{-\delta E/RT} \qquad \text{(eq. 6)}$$

The energetic span is defined as the energy difference between the TDTS (the TOF-determining transition state) and the TDI (the TOF-determining intermediate).

According to the data shown in Table 1 and in Figure 4, following the method described elsewhere,[30] the TDI can be identified as $\mathbf{2_1}$, and the TDTS as $\mathbf{TS1_1}$, being the energy difference between them 26.9 kcal/mol, in good agreement with the experimentally obtained energetic span. However, values calculated using B3LYP/Lanl2DZ (see Table SI3 and a graphical comparison between theoretical levels in Figure SI1, notice that in this case the TDTS is $\mathbf{TS2_1}$ and the TDI is $\mathbf{3_1}$) overestimate the energy span (37.9 *vs* 26.9 kcal/mol) without altering the qualitative energetic description of the process.

The non-catalysed process with three consecutive cycles displays a similar reaction profile than the catalytic one (see Table SI4 and Figures SI2 and SI3 in the Supporting Information). However, a higher energy barrier (56.4 kcal/mol Gibbs free energy in THF at 70 ºC) is required to engage the non-catalysed nitrobenzene reduction. The ratio between the catalysed and non-catalysed processes has been estimated to be $2.52 \cdot 10^{16}$ (in THF at 70 ºC with the data obtained at BP86 level) by using the Eyring-Polanyi equation,[31] thus suggesting an outstanding increase in the rate reaction constant of 16 orders of magnitude in the presence of our molecular cluster catalyst.

Multiple metal centre mechanism

Metal centres in cubane-type Mo_3S_4 cluster act independently, and therefore our calculations have been restricted to a single metal centre as a first approximation. However, formation of cluster species, which result from Mo-H interactions with a second or a third formic acid molecule, cannot be ruled out due to the large excess of the azeotropic $HCOOH/EtN_3$ mixture employed in the experimental catalytic protocol.[7e] As a result, several cluster complexes can be formed, as depicted in Scheme 2. The red arrows correspond to the formation of dihydrogen Mo-H···HOOCH species, abbreviated as Mo-HHfor. The carboxylate ligands (OCHO), formed after substrate reduction, are shown in blue.

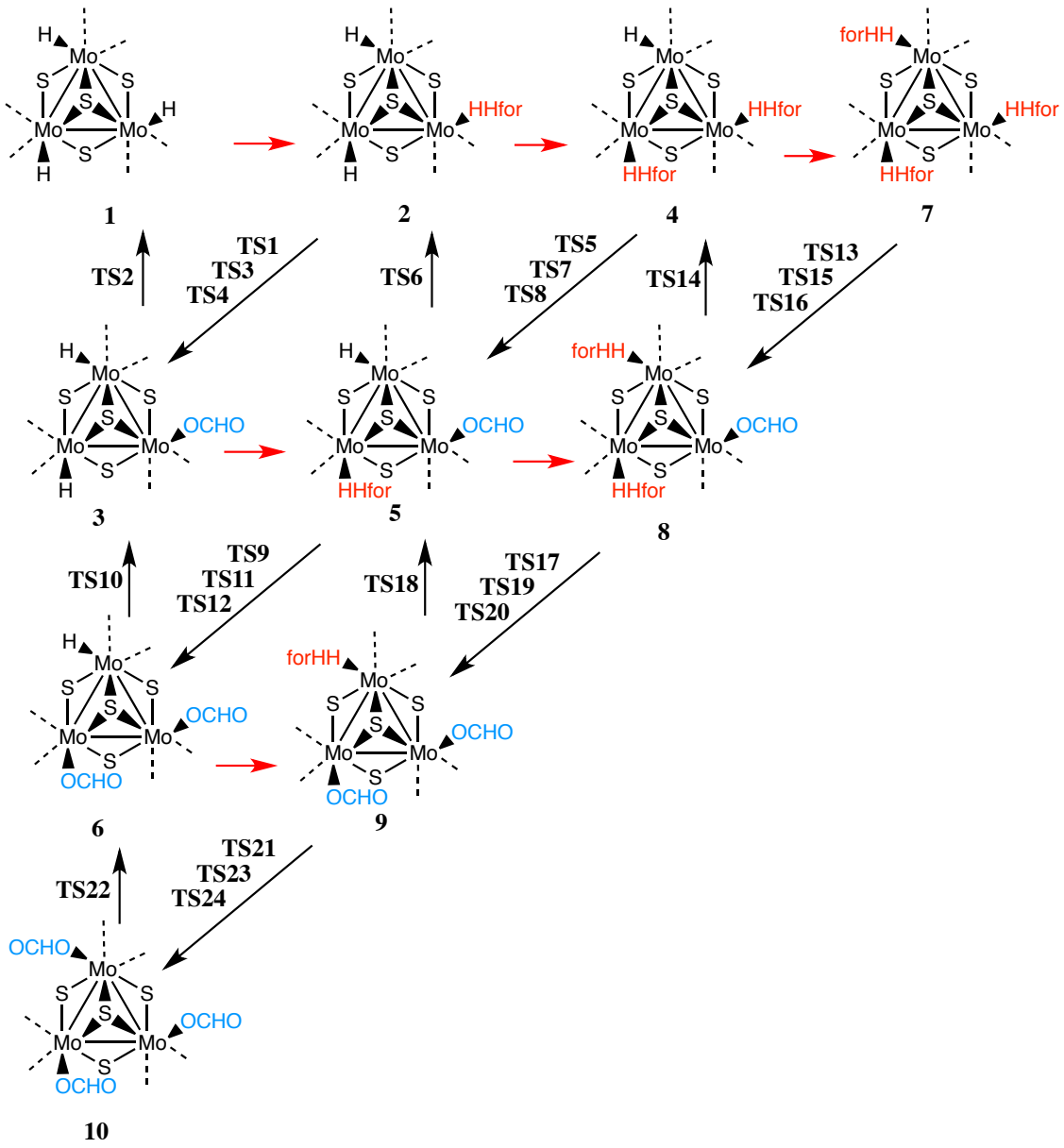

Scheme 2. Different molybdenum cluster species involved in the reduction of nitrobenzene through a multiple metal mechanism.

In the previous section, our study was restricted to the catalytic cycle involving the cluster transformations **1→2→3→1**. However, once **2** is formed (see Scheme 2) the system can incorporate a second HCOOH molecule to form $[Mo_3S_4H_3(PH_3)_6(HOOCH)_2]^+$ (**4**) that, upon reaction with nitrobenzene, affords nitrosobenzene and $[Mo_3S_4H_2(OCHO)(PH_3)_6(HOOCH)]^+$ (**5**), which in turn can regenerate **2** by decarboxylation. In this way a second catalytic cycle can be traced from **2** to **4**, then **5** and back to **2**, and this cycle may continue with the reaction of **4** with nitrosobenzene and afterwards with phenyl hydroxylamine to finally afford aniline. On

the other hand, the formate complex **3** may interact with a HCOOH molecule to give **5** which upon reaction with either nitrobenzene, nitrosobenzene, or phenyl hydroxylamine, evolves to $[Mo_3S_4H(OCHO)_2(PH_3)_6]^+$ (**6**) and upon decarboxylation can go back to **3**. Thus, a third catalytic cycle can then be traced from **3** to **5**, then **6** and back to **3**.

In a similar way, complexes **4**, **5** and **6** can also incorporate HCOOH to form dihydrogen-bonded species through interaction with the third Mo-H bond, thus affording $[Mo_3S_4H_3(PH_3)_6(HOOCH)_3]^+$ (**7**), $[Mo_3S_4H_2(OCHO)(PH_3)_6(HOOCH)_2]^+$ (**8**) and $[Mo_3S_4H(OCHO)_2(PH_3)_6(HOOCH)]^+$ (**9**), respectively. These cluster species can react with either nitrobenzene, nitrosobenzene or phenyl hydroxylamine to trace the new catalytic cycles **4-7-8-4**, **5-8-9-5** and **6-9-10-6**, respectively, **10** being the trisubstituted formate $[Mo_3S_4(OCHO)_3(PH_3)_6]^+$ complex. So, a panoply of catalytic cycles coexist adding complexity to the system and affording a highly efficient catalyst.

The energies of all stationary points calculated at the BP86/BS1 level under experimental conditions are given in Table 2. Structures of selected examples of TSs calculated along the different reaction paths are provided as Supplementary Information (Figure SI3) together with the whole set of Cartesian coordinates for all stationary points. Values obtained from gas phase calculations at room temperature, as well as values calculated at the B3LYP/lanl2DZ level, are also reported as Supplementary Information (Tables SI5 and SI6). In these tables, transitions states have been grouped according to their chemical nature. Thus, **TS1**, **TS5**, **TS13**, **TS9**, **TS17** and **TS21** stand for the transition states corresponding to the reduction of nitrobenzene to nitrosobenzene (TS^a in Table 2). In the same way, **TS3**, **TS7**, **TS15**, **TS11**, **TS19** and **TS23** correspond to the transition states associated with the reduction of nitrosobenzene to phenyl hydroxylamine (TS^b), while **TS4**, **TS8**, **TS16**, **TS12**, **TS20** and **TS24** are the TSs for the reduction of phenyl hydroxylamine to aniline (TS^c). Transition states **TS2**, **TS6**, **TS14**, **TS10**, **TS18** and **TS22** correspond to decarboxylation processes (TS^d).

Table 2. Gibbs free energy variation (ΔG^{*}) for the indicated processes according to Scheme 2, activation barriers ($\Delta G^{\#}$) and subsequent stabilization (ΔG^{sta}) for the indicated TSs. Average activation barriers and standard deviation values are included for each set of TSs. All energies in kcal/mol.*

Process	ΔG^{*}	TS^{a}	$\Delta G^{\#}$	ΔG^{sta}	TS^{b}	$\Delta G^{\#}$	ΔG^{sta}
1→2	1.3	**TS1**	26.9	-58.3	**TS3**	19.1	-52.3
2→4	0.5	**TS5**	26.3	-57.2	**TS7**	17.6	-50.5
4→7	3.5	**TS13**	25.5	-56.9	**TS15**	15.3	-48.6
3→5	0.9	**TS9**	27.6	-57.1	**TS11**	20.7	-52.1
5→8	3.1	**TS17**	25.8	-58.0	**TS19**	18.7	-52.8
6→9	0.4	**TS21**	27.9	-57.0	**TS23**	20.0	-51.0
		Aver.	26.7		**Aver.**	18.5	
		±Std	±0.9		**±Std**	±1.7	
		TS^{c}	$\Delta G^{\#}$	ΔG^{sta}	TS^{d}	$\Delta G^{\#}$	ΔG^{sta}
		TS4	25.7	-93.1	**TS2**	24.1	-17.4
		TS8	29.8	-96.9	**TS6**	24.0	-16.9
		TS16	22.3	-89.7	**TS14**	20.2	-15.6
		TS12	25.4	-91.0	**TS10**	23.4	-18.1
		TS20	23.7	-92.0	**TS18**	24.4	-18.7
		TS24	24.5	-89.7	**TS22**	23.4	-18.0
		Aver.	25.2		**Aver.**	23.2	
		±Std	±2.3		**±Std**	±1.4	

* All calculations have been done in THF at 70 ºC at the BP86/BS1 level.

Activation parameters within each TSs group are rather similar giving support to a statistically controlled kinetics. At the start of the reaction, interaction of cluster **1** with one, two or three molecules of formic acid produces **2**, **4** and **7**, respectively which interact with nitrobenzene through **TS1**, **TS5** or **TS13**, to afford nitrosobenzene and the cluster species **3**, **5** or **8**, respectively. These last two cluster species can also reduce nitrobenzene, through **TS9** or **TS17**, to give **6** or **9**. Complex **9** can in turn reduce nitrobenzene through **TS21.** As soon as nitrosobenzene appears in the reaction mixture, it will compete with nitrobenzene for its catalytic transfer hydrogenation. However, the lower activation barriers calculated for nitrosobenzene hydrogenation (see Table 2, TS^{b} *vs* TS^{a}) causes its

preferential reduction and prevents its accumulation. In this way, nitrosobenzene is a transient intermediate, which is readily transformed to phenyl hydroxylamine. At this point, phenyl hydroxylamine will compete with nitrobenzene for its reduction although phenyl hydroxylamine is preferentially hydrogenated due to the lower activation barriers calculated for the transformation (see Table 2, TS^c *vs* TS^a). Therefore, our results provide a perfectly adequate explanation for the non-accumulation of nitrosobenzene or phenyl hydroxyl amine along the reaction progress.

One can explore different Gibbs free energy profiles to reach the final products, as illustrated in Scheme 2. Starting from **R** (**1** + 3 HCOOH + $C_6H_5NO_2$), and therefore ending at **P** (**1** + 3 CO_2 + 2 H_2O + $C_6H_5NH_2$), the "external" cycle **1-2-4-7-TS13-8-TS19-9-TS24-10-TS22-6-TS10-3-TS2-1** can for instance be traced, being **TS13** the highest energy point. Also, the "zigzag" pathway **1-2-TS1-3-5-TS11-6-9-TS24-10-TS22-6-TS10-3-TS2-1** going through **TS1** as the highest energy point, or the "quasi-external" path **1-2-4-TS5-5-8-TS19-9-TS24-10-TS22-6-TS10-3-TS2-1** with **TS5** as the higher energy transition state, can lead from reactants to products, among many other possibilities. The Gibbs free energies for those three paths are represented in Figure 5 together with values calculated for the "single metal" path.

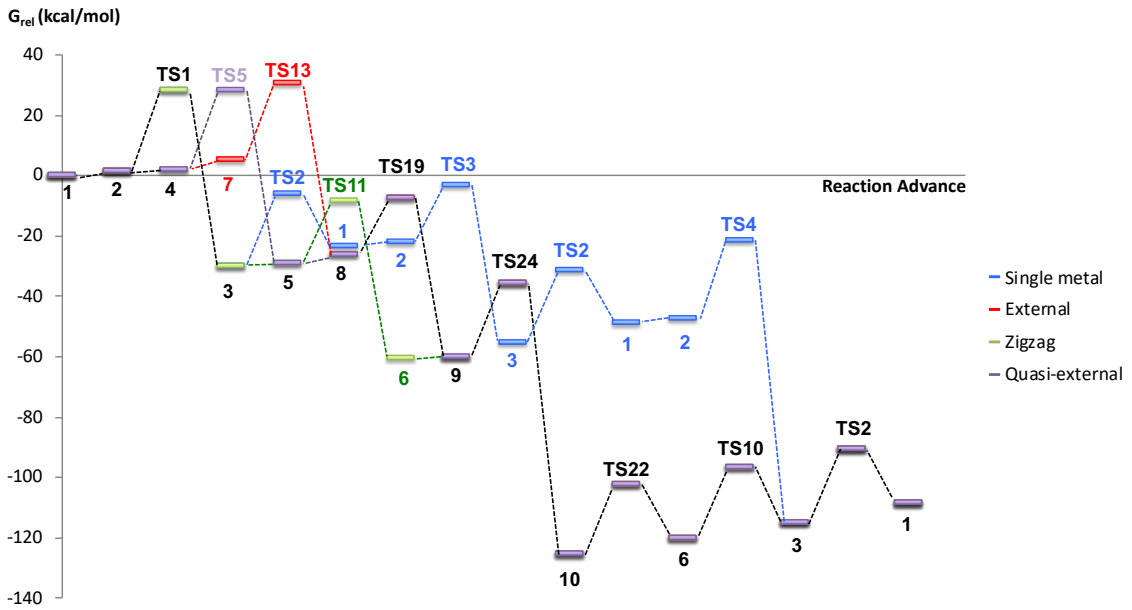

Figure 5. Gibbs free energy profiles (kcal/mol) for several alternative catalytic cycles, calculated at the BP86/BS1 theoretical level in THF at 70 ºC. The black dashed lines correspond to shared paths, while coloured lines refer to particular pathways.

The theoretically calculated energy spans are very similar among this paths, being 25.5 kcal/mol for the "external" path, 26.3 kcal/mol for the "quasi-external" one, and 26.9 kcal/mol for the "zigzag" pathway, as well as for the "single metal" path, and therefore all of them agree with the experimentally obtained energy span. On the other hand, the "quasi-external" path (violet lines in Figure 5) has the lowest energy limiting TS (28.1 kcal/mol Gibbs free energy referred to the reactants for **TS5**) followed by the "zig-zag" (green in Figure 5) mechanism. The Gibbs free energy in this last case is 28.2 kcal/mol (**TS1**), which equals that of the "single metal" mechanism reported in the previous section. The "external path" (red in Figure 5) is slightly disfavoured by 2.8 kcal/mol with a Gibbs free energy for **TS13** of 30.8 kcal/mol. Incidentally, the most favoured "quasi-external" path, as well as the "external" and the "zigzag" paths, go through the most stable intermediates, *i. e.* the tri-substituted formate adduct **10**, and this is the species that is detected by ESI-MS together with the major active hydrido cluster **1** at long reaction times. The small differences among the TSs Gibbs free energies for the different paths indicate that a multiple path mechanism is feasible for the transfer hydrogenation of nitrobenzene catalysed by Mo_3S_4 trinuclear cluster hydrides in the presence of formic acid.

Conclusions

A detailed theoretical investigation using density functional theory has been performed to unravel the mechanism of the transfer hydrogenation to nitroarenes mediated by cubane-type Mo_3S_4 cluster hydrides using an azeotropic HCOOH/Et_3N (5:2) mixture as reducing agent. Our study confirms the formation of Mo-H···HOOCH dihydrogen adducts from which hydrogen is transferred to the different organic substrates. The presence of Et_3N favours the process by reducing the dissociation energy of the formic acid dimers present in THF solutions lowering the energy demand for the generation of this dihydrogen species.

The overall hydrogenation process is highly exergonic and occurs in three consecutive steps with nitrosobenzene and phenyl hydroxylamine as reaction intermediates. All transition states have been identified affording all details related with the hydrogen transfer from the cluster to nitrobenzene, nitrosobenzene and phenyl hydroxylamine.

Initially, our study was restricted to a single metal center, a common simplification in Mo_3S_4 clusters in which their metal atoms reactions follow a statistically controlled kinetics. The highest energy value along this "single metal" reaction path corresponds to **TS1** associated to the nitrobenzene to nitrosobenzene (plus water) transformation. Hydrogen transfer results in the formation of a formate-substituted cluster from which the initial cluster hydride can be regenerated through a β-hydride elimination reaction accompanied by CO_2 release. The energy span estimated from the experimental data is *ca* 25 kcal/mol which agrees with the value of 26.9 kcal/mol calculated at the BP86/BS1 level under the experimental conditions (THF and 70 ºC) in this first approach. Calculations performed at the B3LYP/LanL2DZ level render similar geometries, but energy is overestimated by ca. 15 kcal/mol.

To get a more realistic picture, all possibilities of interaction between formic acid and the three Mo-H moieties have been considered. In this way, we have shown that the cubane-type Mo_3S_4 cluster catalyst evolves along the process and adopts up to ten forms, six of which are activated for catalyzing the process. Computing of all reaction paths starting from each of the ten catalysts forms shows similar TSs energy values with the highest energy associated to the nitrobenzene to nitrosobenzene transformations. Based on this multiple reaction scheme, numerous paths can be envisioned, which confer an outstanding catalytic performance to this type of cluster complexes. The calculated energy span for the so called "multi-metal external path" of 25.5 kcal/mol is in slightly better agreement with the experimental value of *ca.* 25 kcal/mol than the one obtained by means of the "single metal" pathway. The small differences in energies calculated between the single-metal and the multi-metal reaction paths give support to the original idea of a statistically controlled kinetics. However, our study reveals the complex nature of the nitrobenzene to aniline reduction catalyzed by this cluster that works as a highly efficient catalytic machine adopting different forms as the reaction takes place.

We have described only four possible routes, but with the data we offer in Table 2 the readers can test all other paths. Since our theoretical results are in agreement with the available experimental data, we are confident in our theoretical model, that can be generalized to other catalytic systems involving multi-metal centres. We are convinced that this study can stimulate further experimental and theoretical investigations not only on this important class of cubane-type Mo_3S_4 cluster catalysts, but also in other catalytic systems involving multi-metal centres.

Acknowledgments

The authors are grateful to Generalitat Valenciana for PrometeoII/2014/022 and for ACOMP/2015/1202, to Universitat Jaume I for projects UJI-B2016-25 and UJI-B2017-44, and to Ministerio de Economía y Competitividad (Spain) for project CTQ2015-65207-P. I. S. thanks Spanish MINECO for a postdoctoral "Juan de la Cierva-Incorporación" fellowship. The authors also thank the Servei d'Informàtica, Universitat Jaume I, for generous allocation of computer time.

References

1 (a) N. Ono, *in The Nitro Group in Organic Synthesis*, Wiley-VCH, New York, 2001; (b) H. A. Wittcoff, B. G. Reuben and J. S. Plotkin, *in Industrial Organic Chemicals* Wiley-Interscience New York, 2nd edn., 2004; (c) S. A. Lawerencem, *in Amines: Synthesis, Properties and Applications* Cambridge University Cambridge, 2004; (d) D. Formenti, F. Ferretti, F. K. Scharnagl and M. Beller, *Chem. Rev.*, 2018, DOI: 10.1021/acs.chemrev.8b00547.

2 (a) A. Bhattacharya, V. C. Purohit, V. Suarez, R. Tichkule, G. Parmer and F. Rinaldi, *Tetrahedron Lett.*, 2006, **47**, 1861-1864; (b) R. Joncour, N. Duguet, E. Metay, A. Ferreira and M. Lemaire, *Green Chem.*, 2014, **16**, 2997-3002; (c) I. Sorribes, L. Liu and A. Corma, *Acs Catal.*, 2017, **7**, 2698-2708.

3 J. Song, Z.-F. Huang, L. Pan, K. Li, X. Zhang, L. Wang and J.-J. Zou, *Appl. Catal., B*, 2018, **227**, 386-408.

4 (a) E. G. Chepaikin, M. L. Khidekel, V. V. Ivanova, A. I. Zakhariev and D. M. Shopov, *J. Mol. Catal.*, 1980, **10**, 115-119; (b) C. J. Casewit, D. E. Coons, L. L. Wright, W. K. Miller and M. R. DuBois, *Organometallics*, 1986, **5**, 951-955; (c) S. G. Harsy, *Tetrahedron*, 1990, **46**, 7403-7412; (d) S. Xu, X. Xi, J. Shi and S. Cao, *J. Mol. Catal. A: Chem.*, 2000, **160**, 287-292; (e) A. Toti, P. Frediani, A. Salvini, L. Rosi and C. Giolli, *J. Organomet. Chem.*, 2005, **690**, 3641-3651; (f) A. Corma, C. González-Arellano, M. Iglesias and F. Sánchez, *Appl. Catal., A*, 2009, **356**, 99-102; (g) A. A. Deshmukh, A. K. Prashar, A. K. Kinage, R. Kumar and R. Meijboom, *Ind. Eng. Chem. Res.*, 2010, **49**, 12180-12184; (h) G. Wienhofer, M. Baseda-Kruger, C. Ziebart, F. A. Westerhaus, W. Baumann, R. Jackstell, K. Junge and M. Beller, *Chem. Commun.*, 2013, **49**, 9089-9091; (i) E. Pedrajas, I. Sorribes, A. L. Gushchin, Y. A. Laricheva, K. Junge, M. Beller and R. Llusar, *Chemcatchem*, 2017, **9**, 1128-1134.

5 (a) U. Siegrist, P. Baumeister, H.-U. Blaser and M. Studer, *Chem. Ind. (Dekker)*, 1998, **75**, 207-219; (b) A. Corma and P. Serna, *Science*, 2006, **313**, 332-334; (c) M. Boronat, P. Concepción, A. Corma, S. González, F. Illas and P. Serna, *J. Am. Chem. Soc.*, 2007, **129**, 16230-16237; (d) A. Corma, P. Concepción and P. Serna, *Angew. Chem. Int. Ed.*, 2007, **46**, 7266-7269; (e) A. Corma, P. Serna, P. Concepcion and J. J. Calvino, *J. Am. Chem. Soc.*, 2008, **130**, 8748-8753; (f) P. Serna, P. Concepción and A. Corma, *J. Catal.*, 2009, **265**, 19-25; (g) H.-U.

Blaser, H. Steiner and M. Studer, *Chemcatchem*, 2009, **1**, 210-221; (h) K.-i. Shimizu, Y. Miyamoto, T. Kawasaki, T. Tanji, Y. Tai and A. Satsuma, *J. Phys. Chem. C*, 2009, **113**, 17803-17810; (i) K.-i. Shimizu, Y. Miyamoto and A. Satsuma, *J. Catal.*, 2010, **270**, 86-94; (j) P. Serna, M. Boronat and A. Corma, *Top. Catal.*, 2011, **54**, 439-446; (k) T. Mitsudome, Y. Mikami, M. Matoba, T. Mizugaki, K. Jitsukawa and K. Kaneda, *Angew. Chem. Int. Ed.*, 2012, **51**, 136-139; (l) Y. Matsushima, R. Nishiyabu, N. Takanashi, M. Haruta, H. Kimura and Y. Kubo, *J. Mater. Chem.*, 2012, **22**, 24124-24131; (m) M. Makosch, W.-I. Lin, V. Bumbalek, J. Sa, J. W. Medlin, K. Hungerbuehler and J. A. van Bokhoven, *Acs Catal.*, 2012, **2**, 2079-2081; (n) F. A. Westerhaus, R. V. Jagadeesh, G. Wienhoefer, M.-M. Pohl, J. Radnik, A.-E. Surkus, J. Rabeah, K. Junge, H. Junge, M. Nielsen, A. Brueckner and M. Beller, *Nat. Chem.*, 2013, **5**, 537-543; (o) R. V. Jagadeesh, A.-E. Surkus, H. Junge, M.-M. Pohl, J. Radnik, J. Rabeah, H. Huan, V. Schuenemann, A. Brueckner and M. Beller, *Science*, 2013, **342**, 1073-1076; (p) H. Wei, X. Liu, A. Wang, L. Zhang, B. Qiao, X. Yang, Y. Huang, S. Miao, J. Liu and T. Zhang, *Nat. Commun.*, 2014, **5**, 5634; (q) S. Furukawa, Y. Yoshida and T. Komatsu, *Acs Catal.*, 2014, **4**, 1441-1450; (r) P. Lara and K. Philippot, *Catal. Sci. Technol.*, 2014, **4**, 2445-2465; (s) P. Serna and A. Corma, *Acs Catal.*, 2015, **5**, 7114-7121; (t) Z. Wei, J. Wang, S. Mao, D. Su, H. Jin, Y. Wang, F. Xu, H. Li and Y. Wang, *Acs Catal.*, 2015, **5**, 4783-4789; (u) T. Schwob and R. Kempe, *Angew. Chem. Int. Ed.*, 2016, **55**, 15175-15179; (v) X. Wang and Y. Li, *J. Mol. Catal. A: Chem.*, 2016, **420**, 56-65; (w) B. Chen, F. Li, Z. Huang and G. Yuan, *ChemCatChem*, 2016, **8**, 1132-1138; (x) D. Formenti, C. Topf, K. Junge, F. Ragaini and M. Beller, *Catal. Sci. Technol.*, 2016, **6**, 4473-4477; (y) P. Loos, H. Alex, J. Hassfeld, K. Lovis, J. Platzek, N. Steinfeldt and S. Huebner, *Org. Process Res. Dev.*, 2016, **20**, 452-464; (z) L. Liu, P. Concepción and A. Corma, *J. Catal.*, 2016, **340**, 1-9; (aa) J. Nianming, L. Zelong, X. Chungu and L. Jianhua, *ChemistrySelect*, 2017, **2**, 4545-4556; (ab) L. Liu, F. Gao, P. Concepción and A. Corma, *J. Catal.*, 2017, **350**, 218-225; (ac) Z. Wei, S. Mao, F. Sun, J. Wang, B. Mei, Y. Chen, H. Li and Y. Wang, *Green Chem.*, 2018, **20**, 671-679; (ad) R. Millán, L. Liu, M. Boronat and A. Corma, *J. Catal.*, 2018, **364**, 19-30.

6 (a) S. Gladiali and G. Mestroni, in *Transition Metals for Organic Synthesis*, eds. M. Beller and C. Bolm, Wiley-VCH, Weinheim, 2004, p. 145; (b) S. Gladiali and E. Alberico, *Chem. Soc. Rev.*, 2006, **35**, 226-236; (c) J. S. M. Samec, J. E. Backvall, P. G. Andersson and P. Brandt, *Chem. Soc. Rev.*, 2006, **35**, 237-248; (d) X. Liu, S. Li, Y. Liu and Y. Cao, *Chin. J. Catal.*, 2015, **36**, 1461-1475; (e) D. Wang and D. Astruc, *Chem. Rev.*, 2015, **115**, 6621-6686.

7 (a) I. Hideaki, N. Takeshi and F. Kazuo, *Chem. Lett.*, 1976, **5**, 655-656; (b) W. Yoshihisa, O. Tetsuo, T. Yasushi, H. Takao and T. Yasuo, *Bull. Chem. Soc. Jpn.*, 1984, **57**, 2440-2444; (c) A. B. Taleb and G. Jenner, *J. Mol. Catal.*, 1994, **91**, L149-L153; (d) G. Wienhoefer, I. Sorribes, A. Boddien, F. Westerhaus, K. Junge, H. Junge, R. Llusar and M. Beller, *J. Am. Chem. Soc.*, 2011, **133**, 12875-12879; (e) I. Sorribes, G. Wienhoefer, C. Vicent, K. Junge, R. Llusar and M. Beller, *Angew. Chem. Int. Ed.*, 2012, **51**, 7794-7798; (f) G. Wienhoefer, F. A. Westerhaus, R. V. Jagadeesh, K. Junge, H. Junge and M. Beller, *Chem. Commun.*, 2012, **48**, 4827-4829; (g) G. Wienhoefer, F. A. Westerhaus, K. Junge and M. Beller, *J. Organomet. Chem.*, 2013, **744**, 156-159; (h) X.-H. Li, Y.-Y. Cai, L.-H. Gong, W. Fu, K.-X. Wang, H.-L. Bao, X. Wei and J.-S. Chen, *Chem. Eur. J.*, 2014, **20**, 16732-16737; (i) M. Vilches-Herrera, S. Werkmeister, K. Junge, A. Borner

and M. Beller, *Catal. Sci. Technol.*, 2014, **4**, 629-632; (j) J. Tuteja, S. Nishimura and K. Ebitani, *RSC Adv.*, 2014, **4**, 38241-38249; (k) L. Yu, Q. Zhang, S.-S. Li, J. Huang, Y.-M. Liu, H.-Y. He and Y. Cao, *Chemsuschem*, 2015, **8**, 3029-3035; (l) B. Karimi, F. Mansouri and H. Vali, *Chempluschem*, 2015, **80**, 1750-1759; (m) R. V. Jagadeesh, K. Natte, H. Junge and M. Beller, *Acs Catal.*, 2015, **5**, 1526-1529; (n) L. Jiang and Z. Zhang, *Int. J. Hydrogen Energy*, 2016, **41**, 22983-22990; (o) C. Zhang, X. Wang, M. Li, Z. Zhang, Y. Wang, R. Si and F. Wang, *Chin. J. Catal.*, 2016, **37**, 1569-1577; (p) K. J. Datta, A. K. Rathi, M. B. Gawande, V. Ranc, G. Zoppellaro, R. S. Varma and R. Zboril, *Chemcatchem*, 2016, **8**, 2351-2355; (q) T. B. Nguyen, L. Ermolenko and A. Al-Mourabit, *Green Chem.*, 2016, **18**, 2966-2970; (r) C. Yu, X. Guo, Z. Xi, M. Muzzio, Z. Yin, B. Shen, J. Li, C. T. Seto and S. Sun, *J. Am. Chem. Soc.*, 2017, **139**, 5712-5715; (s) L. Jiang, P. Zhou, Z. Zhang, S. Jin and Q. Chi, *Ind. Eng. Chem. Res.*, 2017, **56**, 12556-12565; (t) K. Chaiseeda, S. Nishimura and K. Ebitani, *ACS Omega*, 2017, **2**, 7066-7070; (u) S. Cheng, N. Shang, X. Zhou, C. Feng, S. Gao, C. Wang and Z. Wang, *New J. Chem.*, 2017, **41**, 9857-9865; (v) B. Diganta and S. Lakshi, *ChemistrySelect*, 2017, **2**, 6350-6358.

8 (a) R. Adams and F. A. Cotton, *in Catalysis by Di- and Polynuclear Metal Cluster Complexes*, Wiley-VCH, New York, 1998; (b) P. Braunstein, L. A. Oro and P. R. Raithby, *in Metal Clusters in Chemistry*, Wiley-VCH, Weinheim, 1999; (c) H. Seino and M. Hidai, *Chem. Sci.*, 2011, **2**, 847-857; (d) L. Liu and A. Corma, *Chem. Rev.*, 2018, **118**, 4981-5079.

9 (a) E. Pedrajas, I. Sorribes, K. Junge, M. Beller and R. Llusar, *Chemcatchem*, 2015, **7**, 2675-2681; (b) E. Pedrajas, I. Sorribes, K. Junge, M. Beller and R. Llusar, *Green Chem.*, 2017, **19**, 3764-3768; (c) E. Pedrajas, I. Sorribes, E. Guillamon, K. Junge, M. Beller and R. Llusar, *Chem. Eur. J.*, 2017, **23**, 13205-13212.

10 M. G. Basallote, M. Feliz, M. J. Fernández-Trujillo, R. Llusar, V. S. Safont and S. Uriel, *Chem. Eur. J.*, 2004, **10**, 1463-1471.

11 M. J. Frisch, G. W. Trucks, H. B. Schlegel, G. E. Scuseria, M. A. Robb, J. R. Cheeseman, G. Scalmani, V. Barone, B. Mennucci, G. A. Petersson, H. Nakatsuji, M. Caricato, X. Li, H. P. Hratchian, A. F. Izmaylov, J. Bloino, G. Zheng, J. L. Sonnenberg, M. Hada, M. Ehara, K. Toyota, R. Fukuda, J. Hasegawa, M. Ishida, T. Nakajima, Y. Honda, O. Kitao, H. Nakai, T. Vreven, J. A. Montgomery, Jr., J. E. Peralta, F. Ogliaro, M. Bearpark, J. J. Heyd, E. Brothers, K. N. Kudin, V. N. Staroverov, R. Kobayashi, J. Normand, K. Raghavachari, A. Rendell, J. C. Burant, S. S. Iyengar, J. Tomasi, M. Cossi, N. Rega, N. J. Millam, M. Klene, J. E. Knox, J. B. Cross, V. Bakken, C. Adamo, J. Jaramillo, R. Gomperts, R. E. Stratmann, O. Yazyev, A. J. Austin, R. Cammi, C. Pomelli, J. W. Ochterski, R. L. Martin, K. Morokuma, V. G. Zakrzewski, G. A. Voth, P. Salvador, J. J. Dannenberg, S. Dapprich, A. D. Daniels, Ö. Farkas, J. B. Foresman, J. V. Ortiz, J. Cioslowski and D. J. Fox, *Journal*, 2010.

12 C. T. Lee, W. T. Yang and R. G. Parr, *Phys. Rev. B*, 1988, **37**, 785-789.

13 T. H. Dunning Jr. and P. J. Hay, *in Modern Theoretical Chemistry*, Ed. H. F. Schaeffer III. Vol 3, , New York, 1976.

14 (a) P. J. Hay and W. R. Wadt, *J. Chem. Phys.*, 1985, **82**, 270-283; (b) W. R. Wadt and P. J. Hay, *J. Chem. Phys.*, 1985, **82**, 284-298; (c) P. J. Hay and W. R. Wadt, *J. Chem. Phys.*, 1985, **82**, 299-310.

15 (a) M. Feliz, R. Llusar, J. Andres, S. Berski and B. Silvi, *New J. Chem.*, 2002, **26**, 844-850; (b) A. G. Algarra, M. G. Basallote, M. Feliz, M. J. Fernández-Trujillo, R. Llusar and V. S. Safont, *Chem. Eur. J.*, 2006, **12**, 1413-1426; (c) C. Vicent, M. Feliz and R. Llusar, *J. Phys. Chem. A*, 2008, **112**, 12550-12558; (d) T. F. Beltrán, J. Á. Pino-Chamorro, M. J. Fernández-Trujillo, V. S. Safont, M. G. Basallote and R. Llusar, *Inorg. Chem.*, 2015, **54**, 607-618.
16 T. van der Wijst, C. F. Guerra, M. Swart and F. M. Bickelhaupt, *Chem. Phys. Lett.*, 2006, **426**, 415-421.
17 A. D. Becke, *Phys. Rev. A*, 1988, **38**, 3098-3100.
18 J. P. Perdew, *Phys. Rev. B*, 1986, **33**, 8822-8824.
19 D. Andrae, U. Häußermann, M. Dolg, H. Stoll and H. Preuß, *Theor. Chim. Acta*, 1990, **77**, 123-141.
20 A. Höllwarth, M. Böhme, S. Dapprich, A. W. Ehlers, A. Gobbi, V. Jonas, K. F. Köhler, R. Stegmann, A. Veldkamp and G. Frenking, *Chem. Phys. Lett.*, 1993, **208**, 237-240.
21 (a) P. C. Hariharan and J. A. Pople, *Theor. Chim. Acta*, 1973, **28**, 213-222; (b) W. J. Hehre, R. Ditchfield and J. A. Pople, *J. Chem. Phys.*, 1972, **56**, 2257-2261.
22 K. Fukui, *J. Phys. Chem.*, 1970, **74**, 4161-4163.
23 (a) S. Miertus, E. Scrocco and J. Tomasi, *Chem. Phys.*, 1981, **55**, 117-129; (b) J. L. Pascual-Ahuir, E. Silla and I. Tunon, *J. Comput. Chem.*, 1994, **15**, 1127-1138.
24 (a) S. Grimme, J. Antony, S. Ehrlich and H. Krieg, *J. Chem. Phys.*, 2010, **132**, 154104; (b) S. Grimme, S. Ehrlich and L. Goerigk, *J. Comput. Chem.*, 2011, **32**, 1456-1465.
25 (a) T. F. Beltran, M. Feliz, R. Llusar, J. A. Mata and V. S. Safont, *Organometallics*, 2011, **30**, 290-297; (b) T. F. Beltran, M. Feliz, R. Llusar, V. S. Safont and C. Vicent, *Eur. J. Inorg. Chem.*, 2013, **2013**, 5797-5805.
26 A. G. Algarra, M. G. Basallote, M. Jesus Fernandez-Trujillo, M. Feliz, E. Guillamon, R. Llusar, I. Sorribes and C. Vicent, *Inorg. Chem.*, 2010, **49**, 5935-5942.
27 K. L. Vikse, M. P. Woods and J. S. McIndoe, *Organometallics*, 2010, **29**, 6615-6618.
28 M. C. Neary and G. Parkin, *Chem. Sci.*, 2015, **6**, 1859-1865.
29 S. Kozuch and S. Shaik, *Acc. Chem. Res.*, 2011, **44**, 101-110.
30 S. Kozuch and J. M. L. Martin, *ChemPhysChem*, 2011, **12**, 1413-1418.
31 H. Eyring and M. Polanyi, *Z. Phys. Chem. B*, 1931, **12**, 279-311.